Electronic Structure of Atomically Precise Graphene Nanoribbons

Pascal Ruffieux,[†,*] Jinming Cai,[†] Nicholas C. Plumb,[‡] Luc Patthey,[‡] Deborah Prezzi,[§] Andrea Ferretti,[§] Elisa Molinari,[§,¶] Xinliang Feng,[⊥] Klaus Müllen,[⊥] Carlo A. Pignedoli,[†] and Roman Fasel[†,¶]

[†]Empa, Swiss Federal Laboratories for Materials Science and Technology, 8600 Dübendorf, Switzerland, [‡]Swiss Light Source, Paul Scherrer Institut, 5232 Villigen, Switzerland, [§]Istituto Nanoscienze, Consiglio Nazionale delle Ricerche, 41125 Modena, Italy, [⊥]Max Planck Institut for Polymer Research, 55128 Mainz, Germany, [∥]Department of Chemistry and Biochemistry, University of Bern, 3012 Bern, Switzerland, and [¶]Physics Dept, University of Modena and Reggio Emilia, 41125 Modena, Italy

ABSTRACT

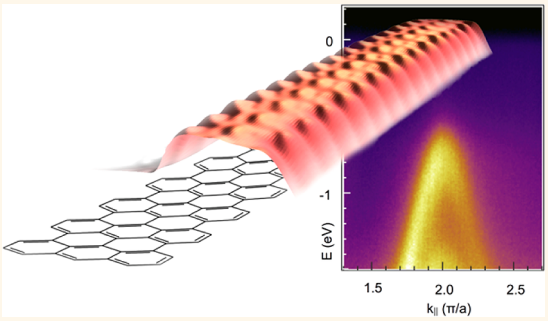

Some of the most intriguing properties of graphene are predicted for specifically designed nanostructures such as nanoribbons. Functionalities far beyond those known from extended graphene systems include electronic band gap variations related to quantum confinement and edge effects, as well as localized spin-polarized edge states for specific edge geometries. The inability to produce graphene nanostructures with the needed precision, however, has so far hampered the verification of the predicted electronic properties. Here, we report on the electronic band gap and dispersion of the occupied electronic bands of atomically precise graphene nanoribbons fabricated *via* on-surface synthesis. Angle-resolved photoelectron spectroscopy and scanning tunneling spectroscopy data from armchair graphene nanoribbons of width $N = 7$ supported on Au(111) reveal a band gap of 2.3 eV, an effective mass of 0.21 m_0 at the top of the valence band, and an energy-dependent charge carrier velocity reaching 8.2×10^5 m/s in the linear part of the valence band. These results are in quantitative agreement with theoretical predictions that include image charge corrections accounting for screening by the metal substrate and confirm the importance of electron–electron interactions in graphene nanoribbons.

KEYWORDS: graphene nanoribbon · electronic structure · effective mass · charge carrier velocity · scanning tunneling spectroscopy · photoelectron spectroscopy · image charge corrections · beyond DFT

The absence of an electronic band gap severely limits the efficiency of graphene-based electronic and optoelectronic switching devices.[1,2] One-dimensional (1D) graphene nanostructures—so-called graphene nanoribbons (GNRs)—have thus attracted much interest due to their semiconducting behavior which is derived from lateral electron confinement.[3−6] A variety of outstanding width and edge-related phenomena emerge from the 1D nature of GNRs, whose properties depend dramatically on the details of the atomic structure.[7−9] GNRs with armchair edges (AGNRs) are expected to exhibit width-dependent electronic band gaps,[4,10] and zigzag GNRs (ZGNRs) are predicted to reveal spin-polarized edge states[11] and half-metallicity[12,13] related to the symmetry breaking between the two atomic sublattices. In addition to straight AGNRs and ZGNRs, more complex ribbon backbone topologies such as in chevron ribbons[14] (also termed "nanowiggles")[9] are predicted to have improved thermoelectric[15,16] and optical[17] properties that are directly related to the non-straight topologies *via* lower thermal conductance and increased spatial localization of the electronic states, respectively. The strong dependence of electronic, thermoelectric, and optical properties on structural details implies that highest precision in GNR fabrication is needed to characterize and exploit such properties. The required atomic precision in GNR fabrication has, however, only very recently been achieved.[14] Here we report on the electronic properties of atomically precise 7-AGNRs (Figure 1A) fabricated *via* on-surface synthesis.[14,18] We take advantage of scanning tunneling spectroscopy (STS)[19] to resolve the local electronic structure and the band gap of the as-grown 7-AGNR. In addition, angle-resolved photoelectron spectroscopy (ARPES)[20] is used to reveal details about the topology of the occupied π-bands of 7-AGNRs.

RESULTS AND DISCUSSION

Spatially resolved recording of tunneling spectra (Figure 1) allows for a clear distinction between substrate-related states and the highest occupied and lowest unoccupied ribbon states (Figure 1B). On the metal, the main contribution to the local density of states (LDOS) is derived from the Shockley surface state of Au(111) with an onset

* Address correspondence to pascal.ruffieux@empa.ch.

Received for review May 1, 2012 and accepted August 1, 2012.

Published online August 01, 2012
10.1021/nn3021376

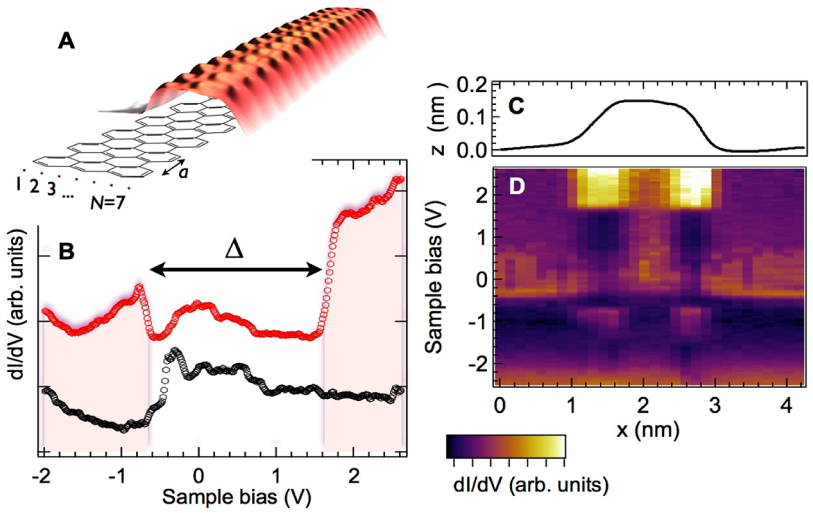

Figure 1. (A) Scanning tunneling microscopy (STM) image ($U = -2.2$ V, $I = 0.15$ nA, 5 K) and chemical structure of an armchair graphene nanoribbon of width $N = 7$ (7-AGNR) on Au(111). (B) Tunneling spectra recorded on the ribbon (red, offset for clarity) and on Au(111) (black). (C) STM line profile across a 7-AGNR. (D) Color-coded representation of 30 dI/dV spectra taken across a 7-AGNR having the ribbon axis at $x \approx 2.1$ nm (tip stabilization parameters: $U = -2.5$ V, $I = 0.2$ nA). Purple corresponds to low intensity; white corresponds to high intensity.

at −0.5 eV below the Fermi energy E_F.[21] In dI/dV spectra taken with the STM tip placed directly above the 7-AGNR, a contribution derived from the surface state is still visible. It appears as a broad and relatively featureless bump between E_F −0.35 eV and E_F +0.7 eV. The corresponding interface state between GNR and the metal surface is upshifted with respect to the Shockley surface state of the clean metal surface due to the modified boundary conditions in the direction normal to the surface, that is, due to the presence of the GNR. Similar characteristic shifts of the Shockley surface state have been observed for adsorbed organic[22] and inorganic layers.[23,24] In such cases, it has been shown that the modified electrostatic boundary conditions confining the state to the surface region lead to substantial energy shifts of the interface state even in the case of overlayers exhibiting significant band gaps.[25] More interestingly, tunneling spectra taken with the tip positioned above the 7-AGNR also show two clear-cut features that appear at E_F −0.7 eV for the occupied states and at E_F +1.6 eV for the unoccupied states. Both clearly mark the onset of 7-AGNR-related electronic bands and are interpreted as the valence band maximum (VBM) and the conduction band minimum (CBM), respectively. From the onset of valence and conduction bands, an electronic band gap of $\Delta = 2.3 \pm 0.1$ eV is derived for the 7-AGNRs supported on a gold substrate.

How does this value compare to the predicted band gap? Electron−electron (e−e) interactions play a dominant role in GNRs due to their quasi-1D nature and the weak screening, as recently shown by state-of-the-art many-body perturbation theory (GW) calculations.[26−28] These effects give rise to an energy gap as large as 3.7 eV for the isolated 7-AGNR,[26,27] significantly larger than

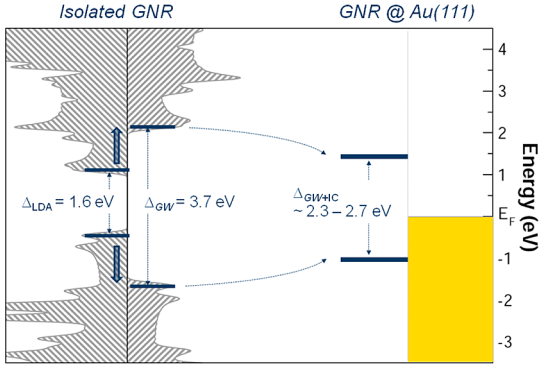

Figure 2. Density of states (DOS) and electronic band gap Δ of the 7-AGNR. Left: LDA and GW-corrected DOS (energy gap Δ highlighted) for the gas phase 7-AGNR. Right: Surface screening, here considered *via* image charge corrections (see text for details), reduces the band gap of the 7-AGNR on Au(111) to 2.3−2.7 eV.

the one predicted by single particle (*e.g.*, tight binding[6] or DFT[4]) approaches (Figure 2). When the ribbon is absorbed on a metal surface, this gap is reduced as an effect of the substrate polarization, which we estimate by including image charge (IC) corrections[29,30] on top of GW calculations for the isolated GNR. Although the molecule/substrate coupling might in general not be limited to polarization effects, this model has been shown to work well for weakly hybridized systems[29−33] because it takes into account the leading order correction. The assumption of a weak interaction between GNRs and the Au(111) substrate is justified by the small hybridization of the electronic bands of ribbons and Au(111) (for details, see the Supporting Information) as well as by the absence of charge transfer and the unperturbed valence band (see ARPES results below). As depicted in Figure 2, GW correction brings the LDA gap of the isolated AGNR from 1.6 to 3.7 ± 0.1 eV.

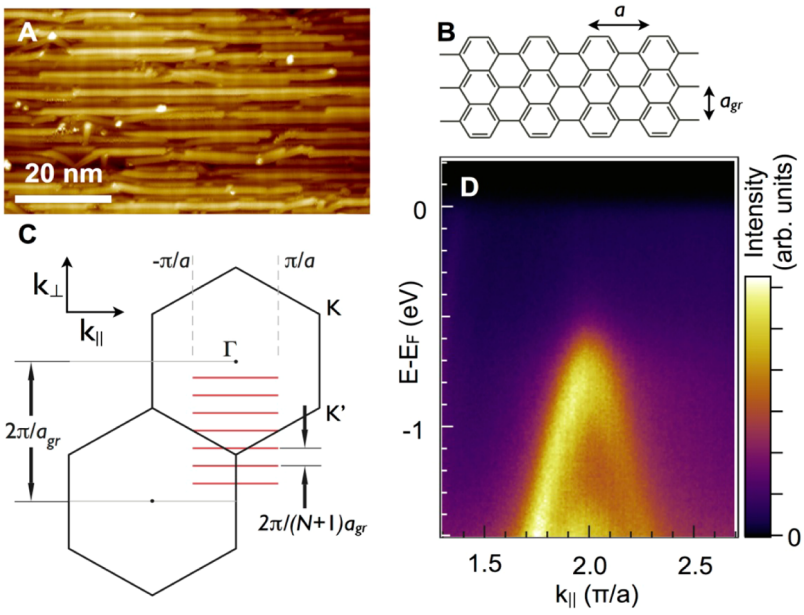

Figure 3. (A) STM image of unidirectionally aligned 7-AGNRs on Au(788) ($U = -1.5$ V, $I = 0.03$ nA, 300 K). (B) Structure of hydrogen-terminated 7-AGNR and relevant lattice parameters. (C) Brillouin zone of graphene (black hexagon) and the one-dimensional Brillouin zone of 7-AGNR (red) with the lattice parameter of AGNRs and a_{gr} the lattice parameter of graphene ($a = a_{gr}$). The transverse wavenumber p is determined by the edge boundary conditions through $p = r\pi/(N + 1)$ with $r = 1,2,...,N$,[40] leading to an interband spacing of $\Delta k_\perp = 2\pi/(N + 1)a_{gr}$. (D) ARPES intensity plot $I(E - E_F,k_{||})$ recorded along the ribbon axis revealing the two occupied frontier bands (raw data, $h\nu = 37$ eV, $T = 300$ K).

The IC correction that mimics the presence of the metallic substrate reduces the energy gap by 1.0−1.4 eV (see Methods). Overall, this results in an energy band gap of 2.3 to 2.7 eV for the 7-AGNR on Au(111), which is in very good agreement with the experimental value of 2.3 ± 0.1 eV derived above.

The band gap detected by STS is not positioned symmetrically with respect to the substrate Fermi level E_F. Qualitatively, this can be understood from the much lower work function of graphene-related materials (4.5−4.6 eV)[34,35] as compared to Au(111) (5.3 eV).[36] Given the weak interaction of GNRs with the Au substrate, one can, in first approximation, assume alignment of the vacuum levels (Schottky−Mott limit),[37] thus suggesting an upward shift of the GNR-related bands with respect to E_F. The experimentally observed upshift is also confirmed by DFT simulations of 7-AGNR adsorbed on Au(111) (Figure S1 in Supporting Information).

Further insight into the occupied electronic states of 7-AGNRs is gained by ARPES (Figure 3). The unidirectional ribbon alignment over macroscopic length scales that is required for k-resolved ARPES measurements has been achieved on regularly stepped gold surfaces, where the long but narrow (few nanometer) (111) terraces confine GNR growth along the terraces (Figure 3A). For higher surface coverages, this leads to a high degree of GNR alignment along step edges running along the substrate [0$\bar{1}$1] direction. ARPES reveals a top of the first 7-AGNR band at E_F −0.7 eV, in agreement with the onset of the valence band

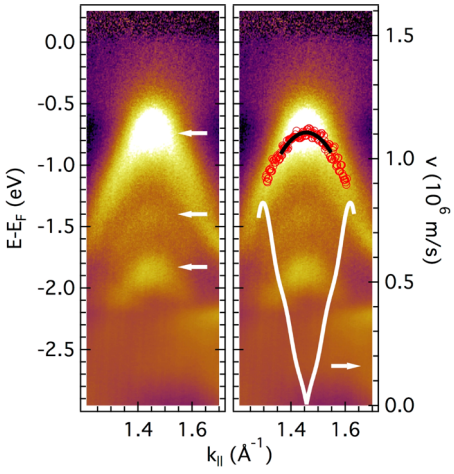

Figure 4. Left: ARPES intensity plots along $k_{||}$ ($h\nu = 50$ eV). The contrast on the GNR-related bands has been enhanced by subtraction of the mean intensity of the momentum distribution curves. The top of the three frontier bands is indicated by arrows at −0.7, −1.4, and −1.8 eV. Right: Valence band peak positions (red circles) extracted from the intensity maxima along the energy dispersive cuts. A parabolic fit to the top of the valence band (energy range 0.17 eV) reveals an effective mass of $m^* = 0.21m_0$. Numerical differentiation of the peak location *versus* $k_{||}$ data reveals the energy-dependent charge carrier velocity v (white, right axis). The corresponding curve has been averaged for the band regions of positive and negative slope and is displayed in a symmetric way with respect to the k-value of the VBM (white, right axis).

observed in STS. The next two bands are located at E_F −1.4 and −1.8 (Figure 4). All of these occupied bands have their maximum at $k = 2\pi/a$ ($a = 0.43$ nm, Figure 3B), which corresponds to the projection of the

K points of the graphene Brillouin zone onto the $k_{||}$ direction for AGNRs (Figure 3C), thus confirming the expected band gap opening at the K points. Furthermore, constant energy k-space mapping confirms the 1D nature of the 7-AGNR dispersion and thus excludes electronic coupling between the GNRs. As a direct consequence of the band gap opening, electrons in AGNRs cannot be considered as massless Dirac Fermions such as in (gapless) graphene,[38,39] but they exhibit a finite effective mass m^*. From a parabolic fit to the top of the valence band, we determine a value of $m^* = 0.21m_0$ (see Figure 4), where m_0 is the free electron mass.

For direct comparison, we have applied an identical parabolic fit (*i.e.*, over the same energy range of 0.17 eV) to the analytic expression describing the valence band of the 7-AGNR using a hopping integral of 2.8 eV.[40] The effective mass derived from this fit is $m^* = 0.21m_0$, in line with experiment. This suggests that AGNRs indeed follow very closely theoretical predictions of their electronic structure, as demonstrated here regarding their electronic band gap and effective electron mass. It must be noted that the effective mass of electrons in GNRs depends strongly on the magnitude of the electronic band gap since the two quantities are intimately related by the dispersion relation of the parent material graphene. For instance, a similar analysis of the analytic description of the valence band of the wider 12-AGNR reveals a much smaller effective mass of $m^* = 0.09$, which is related to its lower band gap of 1.6 eV (GW, in vacuum).[26]

Finally, the ARPES data allow access to another important quantity, namely, the charge carrier velocity $v = 1/\hbar\partial E\partial k$. From the k-dependent peak positions of the valence band (Figure 4), we find that v is energy-dependent and approaches zero at the VBM. This is a direct consequence of the band gap opening and in contrast to the constant velocity $v = v_0 = 10^6$ m/s in graphene. However, for 7-AGNRs, v increases rapidly at lower energies and reaches a maximum velocity of 8.2×10^5 m/s at about 0.5 eV below the VBM.

CONCLUSIONS

We have presented a first experimental characterization of the electronic structure of well-defined AGNRs. ARPES provides a direct confirmation of the predicted gap opening at the K points, and STS gives a band gap of 2.3 eV for the 7-AGNR supported on Au(111). Simple calculations relate the deviation of this value from the predicted 3.7 eV for a free-standing 7-AGNR to screening by the metal substrate. Furthermore, analysis of the ARPES data reveals an effective mass of $0.21m_0$ at the top of the valence band and charge carrier velocities reaching up to ~80% of those in graphene in the linear part of the band, which is in excellent agreement with theoretical predictions. Our results confirm the importance of e−e interactions in GNRs, which lead to significantly larger electronic band gaps than predicted by single particle approaches, and provide an important benchmark for further theoretical and experimental work.

METHODS

Experimental Procedures. 7-AGNRs have been grown on Au(111) as described in ref 14 to yield a coverage of 0.2 monolayers (ML). A similar growth protocol has been adopted for the growth of 7-AGNRs on the stepped Au(788) surface. The metal substrates have been prepared by repeated sputtering/annealing cycles (1 keV Ar^+, 740 K) beforehand. On Au(788), a high degree of GNR alignment is achieved when approaching monolayer coverage. This is due to the confinement of GNRs to the narrow terraces (GNRs avoid to cross substrate step edges) and the optimization of areal density, which is achieved for ribbons aligned along the substrate step edges and packed parallel to each other. Therefore and in order to optimize the ratio between the ribbon- and substrate-related intensity, we chose a coverage of ~0.9 ML for samples to be investigated by angle-resolved photoemission spectroscopy (ARPES).

Scanning tunneling microscopy has been performed at low temperature (low-temperature and variable-temperature STMs from Omicron Nanotechnology GmbH) in constant current mode. The dI/dV spectra have been recorded using the lock-in technique (U_{rms} = 20 mV) at constant tip height.

ARPES measurements have been performed at the Surface and Interface Spectroscopy (SIS) beamline of the Swiss Light Source on samples prepared in the variable-temperature STM chamber and transferred through air. Prior to photoemission experiments, the samples were annealed to 500 K in a UHV chamber connected to the photoemission setup to desorb volatile contaminants accumulated during ambient transfer. STM investigations on samples that were reannealed in the STM setup after the photoemission experiments revealed that substrate and ribbon quality were unaffected by air transfer and photoemission experiments.

Computational Procedures. First principles calculations based on density functional theory (DFT) have been carried out for 7-AGNR, both isolated and on a Au(111) substrate. Calculations have been performed within the local density approximation (LDA) for the exchange-correlation potential, using a plane-wave basis set and ultrasoft pseudopotentials, as implemented in the Quantum-ESPRESSO package.[41] The kinetic energy cutoff for the wave functions (charge density) was set to 25 (300) Ry. The surface was modeled with a five-layer slab of Au(111), using a $3\times4\sqrt{3}$ supercell to accommodate the 7-AGNR; 12 Å of vacuum was added in the direction perpendicular to the slab to avoid spurious interactions with system replicas. The in-plane lattice parameter was set starting from the optimized parameter for bulk Au (4.05 Å), and the atomic positions within the cell were fully relaxed, leading to a GNR−Au(111) mean distance of 3.15 Å.

The GW correction to the LDA energy gap has been taken from previous calculations performed for the isolated 7-AGNR, as described in ref 41. The gap reduction due to the substrate polarization has been estimated by adding the image charge (IC) correction[29,30] to the GW energy gap of the isolated GNR. For simplicity, a uniform distribution of charge was adopted, having a width W = 6.08 Å (average width of 7-AGNR, neglecting H atoms); the distance from the surface was set to the LDA value of 3.15 Å. To avoid the divergence of the IC potential, a screening length L has been defined for the added charge, following Chan *et al.*[42] To estimate this parameter, the spatial extension of lowest bound excitons for the isolated GNR was considered as a lower limit. Previous calculations[41] show this length to be about 30 Å. An upper bound can be estimated considering the

saturation length of the first optical excitation in AGNRs of finite length (*i.e.*, 60 Å).[43] On the basis of the estimated 30−60 Å screening length, an IC correction of 1.0−1.4 eV has been determined.

Conflict of Interest: The authors declare no competing financial interest.

Acknowledgment. We thank J. Krempasky and the beamline technical staff at the Swiss Light Source, Paul Scherrer Institut, for their support. This work is supported by the European Science Foundation (ESF) under the EUROCORES Programme EuroGRAPHENE (GOSPEL), by the Swiss National Science Foundation (SNF), and by the Italian Ministry of University and Research (Grant FIRB-ItalNanoNet to D.P.; Grant FIRB-RBFR08FOAL to A.F.). We acknowledge CINECA and the Swiss National Supercomputing Centre (CSCS) for allocation of computational resources.

Supporting Information Available: Characterization of the 7-AGNR/Au(111) interaction is available as Supporting Information. This material is available free of charge *via* the Internet at http://pubs.acs.org.

REFERENCES AND NOTES

1. Britnell, L.; Gorbachev, R. V.; Jalil, R.; Belle, B. D.; Schedin, F.; Mishchenko, A.; Georgiou, T.; Katsnelson, M. I.; Eaves, L.; Morozov, S. V.; *et al.* Field-Effect Tunneling Transistor Based on Vertical Graphene Heterostructures. *Science* **2012**, *335*, 947–950.
2. Bonaccorso, F.; Sun, Z.; Hasan, T.; Ferrari, A. C. Graphene Photonics and Optoelectronics. *Nat. Photonics* **2010**, *4*, 611–622.
3. Wakabayashi, K.; Fujita, M.; Ajiki, H.; Sigrist, M. Electronic and Magnetic Properties of Nanographite Ribbons. *Phys. Rev. B* **1999**, *59*, 8271–8282.
4. Son, Y.-W.; Cohen, M.; Louie, S. Energy Gaps in Graphene Nanoribbons. *Phys. Rev. Lett.* **2006**, *97*, 216803.
5. Cocchi, C.; Ruini, A.; Prezzi, D.; Caldas, M. J.; Molinari, E. Designing All-Graphene Nanojunctions by Covalent Functionalization. *J. Phys. Chem. C* **2011**, *115*, 2969–2973.
6. Nakada, K.; Fujita, M.; Dresselhaus, G.; Dresselhaus, M. Edge State in Graphene Ribbons: Nanometer Size Effect and Edge Shape Dependence. *Phys. Rev. B* **1996**, *54*, 17954–17961.
7. Wagner, P.; Ewels, C.; Ivanovskaya, V.; Briddon, P.; Pateau, A.; Humbert, B. Ripple Edge Engineering of Graphene Nanoribbons. *Phys. Rev. B* **2011**, *84*, 134110.
8. Cocchi, C.; Prezzi, D.; Ruini, A.; Caldas, M. J.; Molinari, E. Optical Properties and Charge-Transfer Excitations in Edge-Functionalized All-Graphene Nanojunctions. *J. Phys. Chem. Lett.* **2012**, *2*, 1315–1319.
9. Girão, E. C.; Liang, L.; Cruz-Silva, E.; Filho, A. G. S.; Meunier, V. Emergence of Atypical Properties in Assembled Graphene Nanoribbons. *Phys. Rev. Lett.* **2011**, *107*, 135501.
10. Barone, V.; Hod, O.; Scuseria, G. E. Electronic Structure and Stability of Semiconducting Graphene Nanoribbons. *Nano Lett.* **2006**, *6*, 2748–2754.
11. Fujita, M.; Wakabayashi, K.; Nakada, K.; Kusakabe, K. Peculiar Localized State at Zigzag Graphite Edge. *J. Phys. Soc. Jpn.* **1996**, *65*, 1920–1923.
12. Son, Y.; Cohen, M.; Louie, S. Half-Metallic Graphene Nanoribbons. *Nature* **2006**, *444*, 347–349.
13. Lee, Y.-L.; Kim, S.; Park, C.; Ihm, J.; Son, Y.-W. Controlling Half-Metallicity of Graphene Nanoribbons by Using a Ferroelectric Polymer. *ACS Nano* **2010**, *4*, 1345–1350.
14. Cai, J.; Ruffieux, P.; Jaafar, R.; Bieri, M.; Braun, T.; Blankenburg, S.; Muoth, M.; Seitsonen, A. P.; Saleh, M.; Feng, X.; *et al.* Atomically Precise Bottom-Up Fabrication of Graphene Nanoribbons. *Nature* **2010**, *466*, 470–473.
15. Huang, W.; Wang, J. Theoretical Study on Thermoelectric Properties of Kinked Graphene Nanoribbons. *Phys. Rev. B* **2011**, *84*, 045410.
16. Chen, Y.; Jayasekera, T.; Calzolari, A. Thermoelectric Properties of Graphene Nanoribbons, Junctions and Superlattices. *J. Phys.: Condens. Matter* **2010**, *22*, 372202.
17. Wang, S.; Wang, J. Quasiparticle Energies and Optical Excitations in Chevron-Type Graphene Nanoribbon. *J. Phys. Chem. C* **2012**, *116*, 10193–10197.
18. Blankenburg, S.; Cai, J.; Ruffieux, P.; Jaafar, R.; Passerone, D.; Feng, X.; Müllen, K.; Fasel, R.; Pignedoli, C. A. Intraribbon Heterojunction Formation in Ultranarrow Graphene Nanoribbons. *ACS Nano* **2012**, *6*, 2020–2025.
19. Nazin, G. V.; Qiu, X. H.; Ho, W. Visualization and Spectroscopy of a Metal−Molecule−Metal Bridge. *Science* **2003**, *302*, 77–81.
20. Ohta, T.; Bostwick, A.; Mcchesney, J.; Seyller, T.; Horn, K.; Rotenberg, E. Interlayer Interaction and Electronic Screening in Multilayer Graphene Investigated with Angle-Resolved Photoemission Spectroscopy. *Phys. Rev. Lett.* **2007**, *98*, 206802.
21. Chen, W.; Madhavan, V.; Jamneala, T.; Crommie, M. Scanning Tunneling Microscopy Observation of an Electronic Superlattice at the Surface of Clean Gold. *Phys. Rev. Lett.* **1998**, *80*, 1469–1472.
22. Nicoara, N.; Román, E.; Gomez-Rodriguez, J. M.; Martín-Gago, J. A.; Méndez, J. Scanning Tunneling and Photoemission Spectroscopies at the PTCDA/Au(111) Interface. *Org. Electron.* **2006**, *7*, 287–294.
23. Malterre, D.; Kierren, B.; Fagot-Revurat, Y.; Pons, S.; Tejeda, A.; Didiot, C.; Cercellier, H.; Bendounan, A. ARPES and STS Investigation of Shockley States in Thin Metallic Films and Periodic Nanostructures. *New J. Phys.* **2007**, *9*, 391.
24. Park, J.-Y.; Ham, U.; Kahng, S.-J.; Kuk, Y.; Miyake, K.; Hata, K.; Shigekawa, H. Modification of Surface-State Dispersion upon Xe Adsorption: A Scanning Tunneling Microscope Study. *Phys. Rev. B* **2000**, *62*, R16341–R16344.
25. Repp, J.; Meyer, G.; Rieder, K.-H. Snell's Law for Surface Electrons: Refraction of an Electron Gas Imaged in Real Space. *Phys. Rev. Lett.* **2004**, *92*, 036803.
26. Yang, L.; Park, C.-H.; Son, Y.-W.; Cohen, M. L.; Louie, S. G. Quasiparticle Energies and Band Gaps in Graphene Nanoribbons. *Phys. Rev. Lett.* **2007**, *99*, 186801.
27. Prezzi, D.; Varsano, D.; Ruini, A.; Molinari, E. Quantum Dot States and Optical Excitations of Edge-Modulated Graphene Nanoribbons. *Phys. Rev. B* **2011**, *84*, 041401(R).
28. Prezzi, D.; Varsano, D.; Ruini, A.; Marini, A.; Molinari, E. Optical Properties of Graphene Nanoribbons: The Role of Many-Body Effects. *Phys. Rev. B* **2008**, *77*, 041404.
29. Neaton, J. B.; Hybertsen, M. S.; Louie, S. G. Renormalization of Molecular Electronic Levels at Metal−Molecule Interfaces. *Phys. Rev. Lett.* **2006**, *97*, 216405.
30. Thygesen, K. S.; Rubio, A. Renormalization of Molecular Quasiparticle Levels at Metal−Molecule Interfaces: Trends Across Binding Regimes. *Phys. Rev. Lett.* **2009**, *102*, 046802.
31. Tamblyn, I.; Darancet, P.; Quek, S. Y.; Bonev, S.; Neaton, J. Electronic Energy Level Alignment at Metal−Molecule Interfaces with a GW Approach. *Phys. Rev. B* **2011**, *84*, 201402.
32. Dell'Angela, M.; Kladnik, G.; Cossaro, A.; Verdini, A.; Kamenetska, M.; Tamblyn, I.; Quek, S. Y.; Neaton, J. B.; Cvetko, D.; Morgante, A.; *et al.* Relating Energy Level Alignment and Amine-Linked Single Molecule Junction Conductance. *Nano Lett.* **2010**, *10*, 2470–2474.
33. Quek, S. Y.; Venkataraman, L.; Choi, H. J.; Louie, S. G.; Hybertsen, M. S.; Neaton, J. B. Amine-Gold Linked Single-Molecule Circuits: Experiment and Theory. *Nano Lett.* **2007**, *7*, 3477–3482.
34. Ruffieux, P.; Gröning, O.; Bielmann, M.; Mauron, P.; Schlapbach, L.; Gröning, P. Hydrogen Adsorption on sp^2-Bonded Carbon: Influence of the Local Curvature. *Phys. Rev. B* **2002**, *66*, 245416.
35. Yu, Y.-J.; Zhao, Y.; Ryu, S.; Brus, L. E.; Kim, K. S.; Kim, P. Tuning the Graphene Work Function by Electric Field Effect. *Nano Lett.* **2009**, *9*, 3430–3434.
36. Michaelson, H. B. The Work Function of the Elements and Its Periodicity. *J. Appl. Phys.* **1977**, *48*, 4729.
37. Flores, F.; Ortega, J.; Vazquez, H. Modelling Energy Level Alignment at Organic Interfaces and Density Functional Theory. *Phys. Chem. Chem. Phys.* **2009**, *11*, 8658.
38. Novoselov, K.; Geim, A.; Morozov, S.; Jiang, D.; Grigorieva, M.; Dubonos, S.; Firsov, A. Two-Dimensional Gas of

Massless Dirac Fermions in Graphene. *Nature* **2005**, *438*, 197–200.
39. Bostwick, A.; Ohta, T.; Seyller, T.; Horn, K.; Rotenberg, E. Quasiparticle Dynamics in Graphene. *Nat. Phys.* **2007**, *3*, 36–40.
40. Wakabayashi, K.; Sasaki, K.-I.; Nakanishi, T.; Enoki, T. Electronic States of Graphene Nanoribbons and Analytical Solutions. *Sci. Technol. Adv. Mater.* **2010**, *11*, 054504.
41. Giannozzi, P.; Baroni, S.; Bonini, N.; Calandra, M.; Car, R.; Cavazzoni, C.; Ceresoli, D.; Chiarotti, G. L.; Cococcioni, M.; Dabo, I.; *et al.* QUANTUM ESPRESSO: A Modular and Open-Source Software Project for Quantum Simulations of Materials. *J. Phys.: Condens. Matter* **2009**, *21*, 395502.
42. Chan, M. K. Y.; Ceder, G. Efficient Band Gap Prediction for Solids. *Phys. Rev. Lett.* **2010**, *105*, 196403.
43. Cocchi, C.; Prezzi, D.; Ruini, A.; Benassi, E.; Caldas, M. J.; Corni, S.; Molinari, E. Optical Excitations and Field Enhancement in Short Graphene Nanoribbons. *J. Phys. Chem. Lett.* **2012**, *3*, 924–929.